Title
High Resolution Electron Microscopy Study of the Cationic Disorder in Al{sub 2}TiO{sub 5}

Journal
Journal of materials research, 6(1)

Authors
Epicier, T.
Thomas, G.
Wohlfromm, H.
et al.

Publication Date
1989-06-01

LBL-28569
Preprint

Lawrence Berkeley Laboratory

UNIVERSITY OF CALIFORNIA

Materials & Chemical Sciences Division

National Center for Electron Microscopy

Submitted to Journal of Materials Research

High Resolution Electron Microscopy Study of the Cationic Disorder in Al_2TiO_5

T. Epicier, G. Thomas, H. Wohlfromm, and J.S. Moya

June 1989

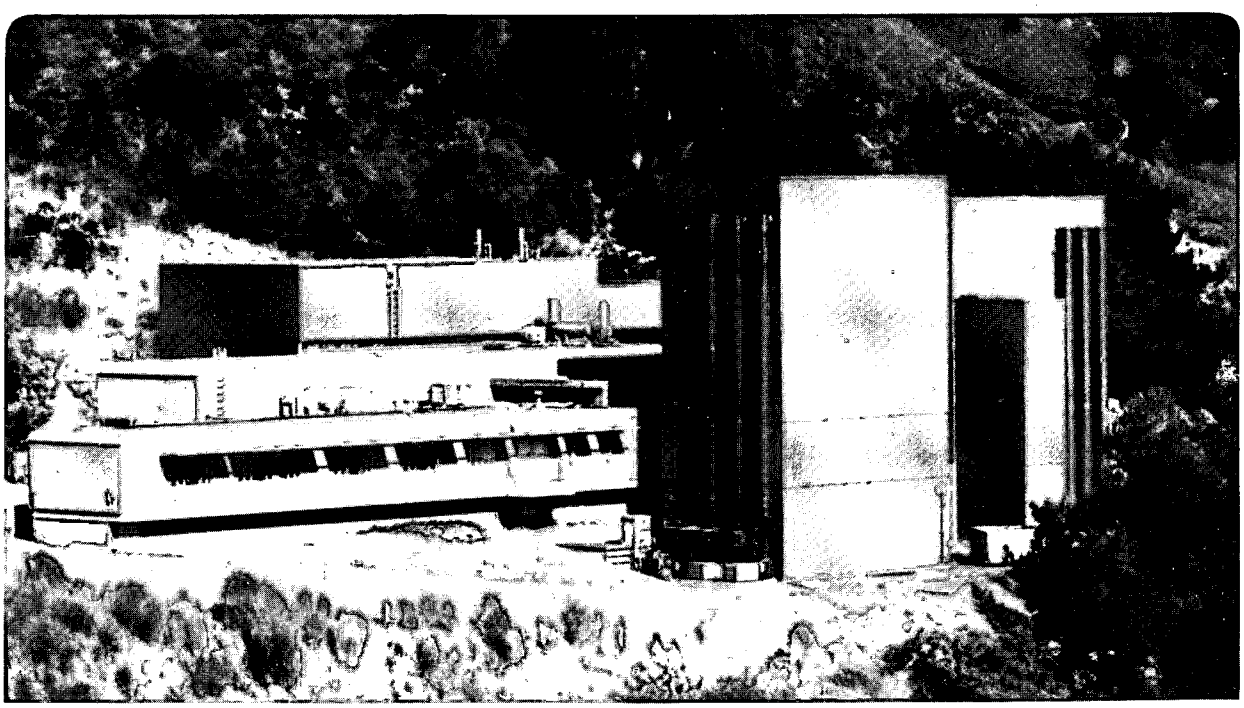

Prepared for the U.S. Department of Energy under Contract Number DE-AC03-76SF00098.

DISCLAIMER

LBL-28569

High Resolution Electron Microscopy Study of the Cationic Disorder in Al_2TiO_5

T. Epicier*, G. Thomas**, H. Wohlfromm+, and J. S. Moya+

**National Center for Electron Microscopy
Materials and Chemical Sciences Division
Lawrence Berkeley Laboratory
University of California
Berkeley, CA 94720

*INSA, GEMPPM, Bat. 502
CNRS 341
69621 Villeurbanne Cedex
France

+Instituto de Ceramica y Vidrio (CSIC)
Arganda del Rey
Madrid, Spain

June 1989

This work was supported by the Director, Office of Energy Research, Office of Basic Energy Sciences, Materials Sciences Division of the U. S. Department of Energy under Contract No. DE-AC03-76SF00098

HIGH RESOLUTION ELECTRON MICROSCOPY STUDY OF THE CATIONIC DISORDER IN Al_2TiO_5

T. Epicier*, G. Thomas, H. Wohlfromm+ , and J. S. Moya+

National Center for Electron Microscopy

Materials and Chemical Science Division, Lawrence Berkeley Laboratory,

1 Cyclotron Road, Berkeley, California 94720 USA

Abstract

As part of a research program devoted to the microstructural characterization of Al_2TiO_5-based compounds, high resolution electron microscopy (HREM) has been undertaken in order to study the crystallographic arrangement, especially ordering possibilities, of Al and Ti cations in the metallic sublattice of aluminium titanate. It is seen that adequate experimental conditions, mainly defocus setting, for a resolution of at least 2.5 Å point-to-point, enable the disordered model to be directly and unambiguously proved on [100]-oriented micrographs.

Introduction

1. Generalities

Aluminium titanate Al_2TiO_5 (tialite) is a synthetic ceramic material of potential interest for many structural applications, owing to its high melting point, low thermal conductivity and excellent thermal shock resistance. However, a critical feature, which greatly limits the mechanical properties of polycrystalline Al_2TiO_5 is considerable intergranular microcracking which occurs due to the high thermal anisotropy of individual grains (orthorhombic β-Al_2TiO_5 with $\alpha_a = -2.9$, $\alpha_b = 10.3$ and $\alpha_c = 20.1\ 10^{-6}\ K^{-1}$ (Bayer, 1971). Another problem arises from the thermodynamical decomposition of Al_2TiO_5 into alumina (Al_2O_3) and rutile (TiO_2) below about 1300°C (Kato, Daimon and Takahashi, 1980). The latter disadvantage

*permanent address : INSA, GEMPPM, Bât. 502, u. a. CNRS 341, 69621 Villeurbanne Cedex, FRANCE.

+ permanent address : Instituto de Ceramica y Vidrio (CSIC), Arganda del Rey (Madrid), SPAIN.

can be overcome by substituing Al, or Al and Ti, by small quantities of Si or Mg ions to form solid solutions which allow the thermal decomposition to be controlled (Ishitsuka, Sato, Endo and Shimada, 1987).

In the course of a general study of various Al_2TiO_5-based compounds (Wohlfromm, Moya and Pena, 1989), a structural investigation of pure and Mg-doped Al_2TiO_5 polycrystals has been performed by means of High Resolution Electron Microscopy (HREM). The aim of this work was mainly to check the crystallographic arrangement of Al and Ti ions on the metallic sublattice of these oxide materials. During this research, it was also possible to characterize the dislocations (Epicier, Wohlfromm and Thomas, 1989).

2. Crystallographic background (Table 1 and Figure 1)

Basic structural studies of Al_2TiO_5 have been done by Hamelin (1957) and Morosin and Lynch (1972). In the former work, X-ray diffraction data were interpreted assuming the space group Bbmm, and assigning Ti ions on fourfold sites and Al ions on eightfold sites (see figure 1 and table 1). However, the relatively large error factor value ($R \approx 17\%$) motivated the latter authors to re-do similar experiments at 20° and 600°C, but assuming a disordered distribution of both types of cations on the same atomic positions; acceptable R values of $\approx 6\%$ were obtained under this condition, supporting the hypothesis of complete cationic disorder.

Since both structures (i.e. ordered and disordered, hereafter labelled O and D) belong to the same space group, with identical atomic positions (leading to the same extinction rules), no superstructure reflection is expected for the O-form compared with the D-one, and the differentiation of both models requires a detailed refinement procedure of diffraction data. Thus, it appears to be useful to investigate this problem using an other technique, viz., HREM.

3. "Chemical analysis at an atomic scale" in HREM

The present approach was also attempted in order to see if HREM can be an efficient tool in obtaining compositional analysis at an atomic scale.

Previous studies have already demonstrated such situations in cases when "superstructure imaging" was permitted by the crystallography of the compounds studied (e.g. when superstructure beams are produced by the ordered distribution of metallic (Hiraga, Shindo and Hirabayashi, 1981, Van Tendeloo, Van Dyck and Amelinckx, 1986) or metalloid (Guan, Hashimoto and Kuo, 1986, Epicier, Blanchin, Ferret and Fuchs, 1989) atoms on adequate sublattices). It is of the greatest importance to know what can be obtained by HREM in the general case where there is no way to image selectively a "mono-element" sublattice, due to the absence of any superlattice reflection. Obviously, the major difficulty of this approach is the frequent requirement of a very good instrumental resolution to allow, at least, the atomic columns to be conveniently separated along adequate azimuths where atomic rows have a unique chemical nature[1]. Then, an instrument from the new generation of "Atomic Resolution Microscopes" (ARM), with a resolution better than 0.2 nm, is generally needed, as elegantly demonstrated by recent works on the polarity of III-V semi-conductors materials (Ourmazd, Rentschler and Taylor, 1986, Glaisher, Spargo and Smith, 1989) and similar approaches on superconducting ceramics (Thomas, Hetherington, O'Keefe, Kilaas, Ramesh and Epicier, 1990).

In the present work, the ARM at the National Center for Electron Microscopy (NCEM) at Berkeley enables this question to be elucidated. However, the resolution requirement is not critical here, since, in the [100] projection of Al_2TiO_5, pure Ti and Al columns in the O-model are largely separated by distances of about 0.25 nm as shown in Figure 1.

---

[1] Although helpful, this geometrical requirement is not compulsory, since reliable contrast modifications may be produced by substitution of a sufficient number of "A" atoms by "B" atoms along a "defective" column (see the basic works by Coene, Van Dyck, Van Landuyt and Amelinckx (1987), and Howe, Basile, Prabhu, Hatalis (1988)).

Experimental procedure

1. Specimen.

Two types of polycrystalline Al_2TiO_5 compounds have been used in the present investigation by sintering of adequate mixtures of Al_2O_3, TiO_2 and MgO powders (Wohlfromm, Moya and Pena, 1989). The first sample (labelled AT100) corresponds to pure aluminium titanate, and the matrix has the following composition:

$$Al_{2\pm0.2}\ Ti_{0.9\pm0.1}\ O_{4.9\pm1}\ Mg_{<0.014}\ Zr_{<0.01}$$

as deduced from chemical analysis in the microscope (see sub-section 2). The second sample (MAT100) has been stabilized by MgO and can be formulated as :

$$Al_{2\pm0.3}\ Ti_{1.1\pm0.2}\ Mg_{0.12\pm0.05}\ O_{5\pm0.2}\ Si_{<0.02}$$

Thin foils were prepared from these materials following classical mechanical and ion-beam (5.5 kV argon beams, incidence angle 30°) thinning procedures. Carbon coating was performed in order to avoid charging under the electron beam in the microscope.

2. Chemical analysis

Chemical analysis of the samples was performed in a JEOL 200 CX microscope, equipped with an ultra-thin window detector and a Kevex 8000 Analyst. Simultaneous analysis of oxygen, aluminium and titanium was conducted on several grains. The data were consistently interpreted after careful thickness measurements were made by convergent-beam diffraction work, in order to allow the absorption correction to be taken into account in the quantitative analysis procedure. The results are given in sub-section 1.

3. HREM observations

The high resolution study was made at 800 kV using the Berkeley ARM. Multislice calculations were conducted with the NCEMSS programs (Kilaas 1987) adopting the crystallographic data reported in Table 1. Other relevant information concerning both operating conditions and required data for simulations are in accordance with those given in Table 2 (Contrast Transfer Functions, CTF, reported hereafter were obtained in the usual way using the data of Table 2). Adequately oriented grains were observed along the [100] azimuth. Digitizing of the micrographs with an Eikonix 78/99 camera controlled by a locally-written command incorporated into the SEMPER programs (Saxton, Pitt and Horner, 1979) was performed for numerical treatment of the experimental images (see next section, § 2).

Results

1. AT100

Figure 2 shows a set of experimental HR images at different defoci, compared to calculated images from both D- and O-models. Careful examination of these images leads to the conclusion that the disordered model produces a better match of the experimental data than does the O-model (see especially images at 15 and -10 nm). Although this result is unambiguous, it may be noted that some of the experimental micrographs do not allow the D- and O-models to be easily distinguished (for example, images at -40 nm, or more clearly, at -100 nm); the reason for this will be discussed in the next section.

2. MAT100

A through-focus series obtained from the Mg-doped compound leads to the same conclusion that the cationic sublattice is disordered. Evidence for this can be illustrated here by a different but complementary approach, consisting of a numerical treatment of an experimental image such as the one shown in Figure 3. In figure 4, intensity profiles across different white dots (corresponding to exact cation column

locations as deduced from the matching image superimposed in Figure 3) are reproduced from experimental and calculated micrographs.

The first set of curves (Fig. 4b) is from the observed image, and was obtained after averaging more than 50 positions in each case. It can be noted that, due to slight misalignment of the electron beam estimated from the matching procedure (≈0.5 mrad, as indicated in the diffraction pattern in Figure 3), intensities corresponding to the equivalent "$4c_1$" and "$4c_2$" columns of 4c-type atoms are not equal ; this does not affect the analysis. However, it is clearly seen that "$4c_1$" and "$8f_2$" (respectively associated to pure titanium and aluminium columns in the ordered model) have almost the same intensity level ; this feature is consistent with the disordered model (Fig. 4c) but does not agree with the ordered model (Fig. 4d).

Discussion and conclusions

1. Explanation of HR contrasts

As already mentioned in the introduction, "chemical analysis at an atomic scale" through careful HREM imaging has become possible due to the excellent resolution performances of modern electron microscopes. The present example illustrates this point, since it has been demonstrated that the disordered distribution of Al and Ti atoms in Al_2TiO_5 is confirmed (at the expense of an ordered arrangement) by detailed imaging with the ARM.

The basic reason allowing such a difference in the chemical nature of atoms to be detected in HREM is the difference in the scattering factor $f(\theta)$ of elementary species (θ is the Bragg angle). The relative scattering power of any atom ($f(\theta)$), and consequently its projected potential, can adequately be described in terms of its atomic number Z. Beyond the peculiarities associated with the crystallographic arrangement, the aluminium/titanium couple is not a difficult case, since their atomic numbers are significantly different, viz. :

$$Z_{Al} = 13, Z_{Ti} = 22$$

In situations utilizing controlled defocus settings and crystal thicknesses where atomic columns are directly imaged, either as dark or white dots, the composition of these atomic columns is simply related to the intensity of the dots. Figure 3 illustrates this simple relation. Due to the low thickness (≈1.4 nm) and the choice of a +10 nm defocus value, which leads to a CTF with a large transmission plateau for spatial frequencies up to ≈$(0.24\ nm)^{-1}$, cationic columns are imaged as white dots; the resulting micrograph can then be considered as a projection of the crystal structure potential with a reverse contrast compared to the classical Scherzer image (e.g., in the present case, white atomic rows). The fact that both "$4c_1$" and "8f" columns have a comparable brightness (as deduced from Figure 4) is a consequence of the random distribution of Al and Ti atoms on the corresponding sites (the ordered case obviously leads to brighter "4c" Ti-columns, due to the stronger Ti scattering power, see inset simulation in Figure 3, and Figure 4d).

A similar situation occurs in the images near the Scherzer condition (defocus value ≈ -55 nm) in the series of Figure 2; although the difference between both D- and O-models is somewhat tedious to detect by eye, a careful examination of the corresponding calculated images shows that "4c" columns are darker in the case of the O-form, e.g. when they are occupied only by the heavier Ti atoms.

From Figure 2, it clearly appears that the Scherzer defocus, which is generally used to obtain the optimal HREM image of any crystalline structure, is not necessarily the best choice to reveal details such as the one discussed here . Indeed, it is seen that the setting of defocus at -10 nm (for instance) provides an easier differentiation of D- and O-forms in the case of Al_2TiO_5, although the corresponding HREM image obviously does not reproduce the exact [100] projection of the crystal.

As far as the weak-phase object approximation is valid (that is, for very thin crystals), such optimal imaging conditions can be determined from an appropriate analysis of the shape of the CTF.

For particular defocus values, it may happen that a plateau (or a zero) of the CTF enhances (or reduces) the transmission of a given spatial frequency (see e.g. Van Tendeloo et al. (1986) and Ourmazd et al. (1986) for applications of these basic ideas). In order to discern the arrangement of cations in Al_2TiO_5, one clearly has to favour the transmission of frequencies corresponding to diffracted beams, the structure factors of which vary as much as possible from the O- to the D-model. Although this explanation is the true reason for the successful differentiation of both models in the images reported in Figure 2, it is not so clear when illustrated by the plots shown in Figure 5. However, these diagrams prove that the prominent beams of similar amplitude in both models (see arrows in Figure 5) are much more efficiently transmitted in the -100 nm defocus case than in the -10 nm defocus case, leading to the observed situation that the different structures are less easily distinguishable in the former image than in the latter one.

2. Conclusion; consequences on the crystal chemistry of Al_2TiO_5

The above results directly confirm the previous X-ray diffraction study of Morosin and Lynch (1972), which claimed a disordered arrangement for Al and Ti cations in Al_2TiO_5. Moreover, our work also shows that the same situation is encountered in Mg-doped aluminium titanate. From this it seems that the well-known stabilizing effect of Al_2TiO_5 by the addition of Mg is due to a reduction of the distortion of atomic coordination polyhedra responsible for the high thermal expansion anisotropy of pure aluminium titanate. In this work, it has not been possible to obtain reliable information on this point, since the structure of the Mg-Al_2TiO_5 solid solution appears to be correctly described with atomic positions equal to those refined in the case of pure aluminium titanate and given in Table 1. In other words, calculated images of MAT100 are already in good agreeement with experimental micrographs without taking into account possible atomic displacements, which must then be very small if existing. Moreover, the random distribution of few

Mg atoms does not lead to significant changes in calculated images compared to those conducted without Mg atoms for the range of thickness explored in this study.

Acknowledgements

It is a great pleasure to acknowledge the assistance of E.C. Nelson and C.J.D. Hetherington in the use of the ARM, and of R. Kilaas and M.A. O'Keefe in the computations. Thanks are due to C. Echer and J. Turner for their respective help in analytical microscopy and image processing. Some financial assistance from Mobil Oil Corporation is also acknowledged. Work at NCEM was supported by the Director, Office of Energy Research, Office of Basic Energy Sciences, Materials Science Division, U.S. Department of Energy under Contract No. DE AC0376SF00098. The support of N.A.T.O. in the form of a Research Fellowship to T.E. is gratefully acknowledged.

References

Bayer G., (1971), *J. Less Com. Metals*, **24** pp. 129-138.

Coene W., Van Dyck D., Van Landuyt J., Amelinckx S., (1987), *Philos. Mag. B*, **56**, 4, pp. 415-427

Epicier T., Blanchin M.G., Ferret P., Fuchs G., (1989), *Philos. Mag. A.*, **59**, 4, pp. 885-906

Epicier T.A., Wohlfromm H., Thomas G., (1989), pp. 422-423 in *Proc. 47th Ann. Meet. EMSA*, San Franciscio Press Inc.

Glaisher R.W., Spargo A.E.G., Smith D.J., (1989), *Ultramicrosc.*, **27**, pp. 19-34

Guan R., Hashimoto H., Kuo K.H., (1986), *Ultramicrosc.*, **20**, pp. 195-202

Hamelin M., (1957), *Congr. Intern. Chim. Pure Appl.*, **16**, p. 151

Hetherington C.J.D., Nelson E.C., Westmacott K.H., Gronsky R., Thomas G. (1989), Mat. Res. Soc., Symp. Proc. **139**, p. 277-282

Hiraga K., Shindo D., Hirabayashi M., (1981), *J. Appl. Cryst.*, **14** , pp. 169-190

Howe J.M., Basile D.P., Prabhu N., Hatalis M.K., (1988), *Acta Cryst.*, **A44**, pp. 449-461

Ishitsuka M., Sato T., Endo T., Shimada M., (1987), *J. Am. Ceram. Soc.*, **70**, 2, pp. 69-71

Kato E., Daimon K., Takahashi J., (1980), *J. Am. Ceram. Soc.*, **63**, 5, pp. 355-356

Kilaas R., (1987), pp. 66-69 in *Proc. 45th Ann. Meeting EMSA*, San Francisco: G.W. Bailey

Morosin B., Lynch R.W., (1972), *Acta Cryst.*, **B28**, pp. 1040-1046

Ourmazd A., Rentschler J.R., Taylor D.W., (1986), *Phys. Rev. Letters*, **57**, 24, pp. 3073-3076

Saxton W.O., Pitt T.J., Horner M., *Ultramicrosc.* **4** (1979), pp 343

Thomas G., Hetherington C.J.D., O'Keefe M.A., Kilaas R., Ramesh R., Epicier T., (1990), to appear in *Proceed. Mat. Res. Soc. Spring Meet.*, (San Franscisco, USA)

Van Tendeloo G., Van Dyck D., Amelinckx S., (1986), *Ultramicrosc.*, **19**, pp. 235-252

Wohlfromm H., Moya J.S., Pena P., (1989), submitted to *J. of Mat. Sci.*

TABLE 1

space group Cmcm

a=0.3591 nm

b=0.9429 nm

c=0.9636 nm

atom	designation	x	y	z	occupancy	Debye-Waller (nm^2)
Ti	(4c)	0	0.1863	0.25	1	0.0111
Al	(8f)	0	0.1351	0.5613	1	0.001
O	O_1 (4c)	0	0.759	0.25	1	0.009
O	O_2 (8f)	0	0.048	0.118	1	0.006
O	O_3 (8f)	0	0.317	0.075	1	0.009

Table 1: crystallographic data concerning the ordered form of Al_2TiO_5 (the disordered form is obtained through a random distribution of Ti and Al atoms on the same (4c) and (8f) sites). The data have been harmonized from Hamelin (1957) and Morosin and Lynch (1972), which however described the crystal in the equivalent space group Bbmm.

TABLE 2

.accelerating voltage:.....800 kV
.spherical aberration coefficent C_S:.....2 mm*
.spread of focus:.....15 nm*
.semi-angle of beam convergence:.....0.8 mrad**
.objective aperture radius:.....8.9 nm^{-1}
.maximal spatial frequency for the multislice beam :..20.0 nm^{-1} (512 beams)
.maximal spatial frequency for the multislice phasegrating:.....40.0 nm^{-1} (2050 coeffs)
.thickness of the elementary slice:.....0.359 nm (|a|)
.crystallographic data:.....as in table 1

* in agreement with actual values determined by Hetherington, Nelson, Gronsky, Westmacott and Thomas (1988). Under such conditions, the "point resolution" of the microscope appears to be limited to 0.16 nm, due to the chromatic error and residual vibration (the "Scherzer resolution limit" would be around 0.14 nm)

** experimentally measured on diffraction patterns.

Table 2: experimental and computing data for the HREM work.

FIGURE CAPTIONS

Figure 1: [100] projection of Al_2TiO_5 (ordered cell).

Figure 2: HREM analysis of AT100 ([100] projection). The micrograph on the left (a) was taken at a defocus of -45 ± 5 nm, as deduced from the inset diffractogram. The "matrix" of images corresponds to various defocus values (from top to bottom : +15, -10, -20, -30, -40 and -100 nm-- images at +15 and -40 nm reveal cation columns as bright and dark dots respectively). The three columns of images correspond respectively to experimental micrographs (b), and simulated images (c, d) calculated from the D- and O-models at a thickness of 4 nm.

Figure 3: HREM [100] micrograph (from a through-focus series not reported here of MAT100 (thickness ≈ 1.4 nm, defocus value = 10 nm--see inset diffractogram). Matching simulated images for both disordered and ordered models have been superimposed on the experimental micrograph. The slight beam misalignment is indicated by the cross in the diffraction pattern, which spots the position of the optical axis.

Figure 4: Numerical treatment of the experimental micrograph from Figure 3. a) detail from Fig. 3 showing the lines X_i-Y_i (i=1,3) followed for intensity profiles plotted in b). Atomic columns are labelled with the name of corresponding Wyckoff atomic positions. b) Intensity profiles from the experimental image (after averaging); note the similitude of "$4c_1$" and "$8f_2$" profiles. c), d) Similar intensity profiles from calculated images for the D- and O-models respectively (the slight disagreement in the low intensity details between b) and c), d) results from the non-normalization of the initial grey levels, and the averaging of numerous positions in the experimental micrograph).

Figure 5: CTF at -100 (a) and -10 nm (b) with superimposition of structure factor histograms for both D- and O-models (respectively dotted and full lines plotte in the positive and negative parts of the diagrams to allow the manner in which each beam is modulated by the CTF to be more conveniently visualized).

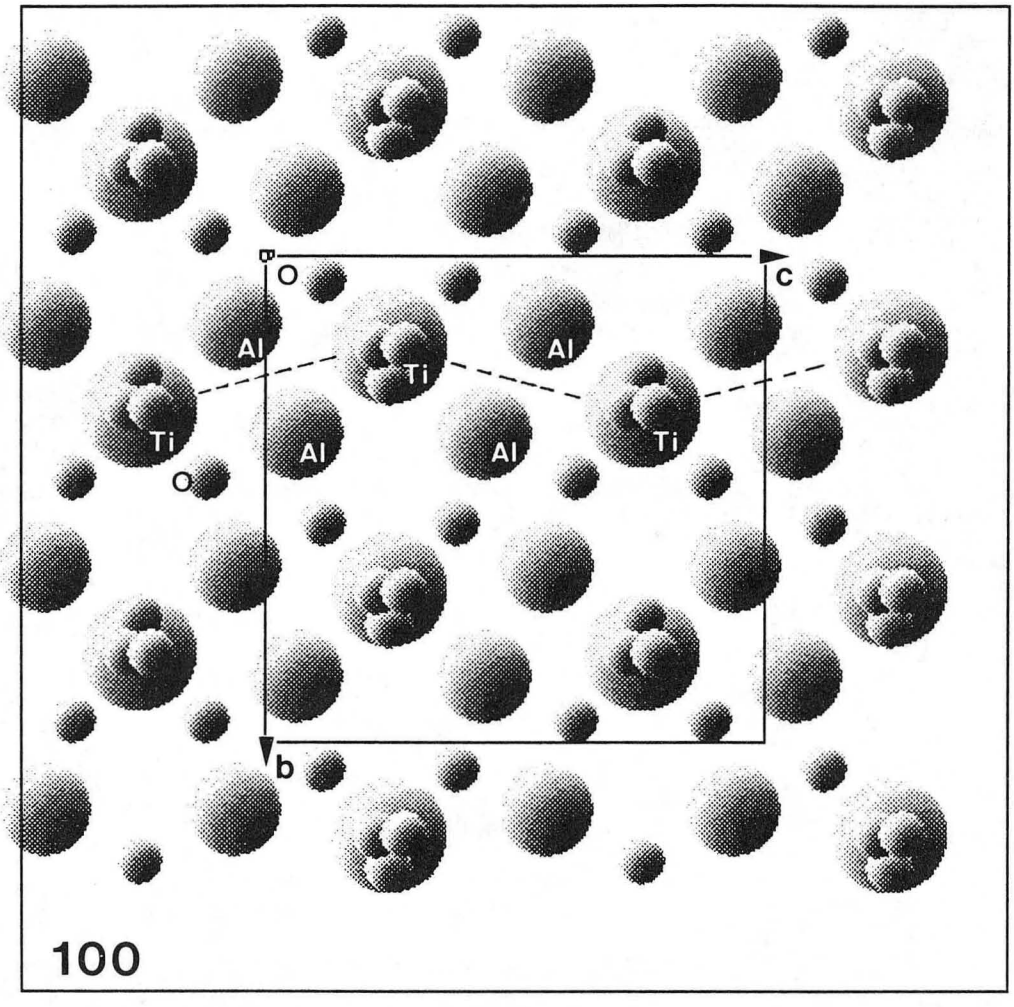

XBL 893-947

Fig. 1

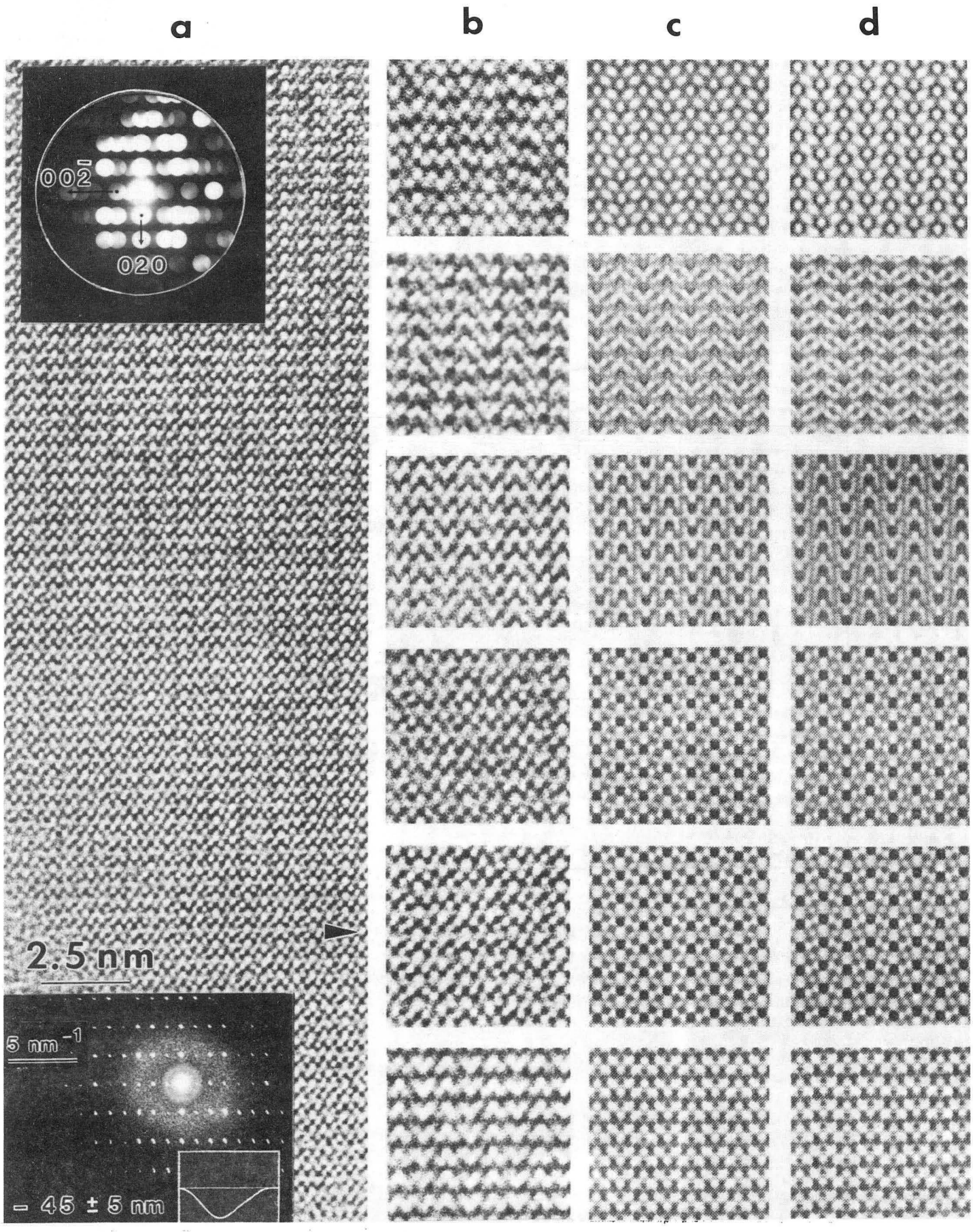

Fig. 2

XBB 902-1487

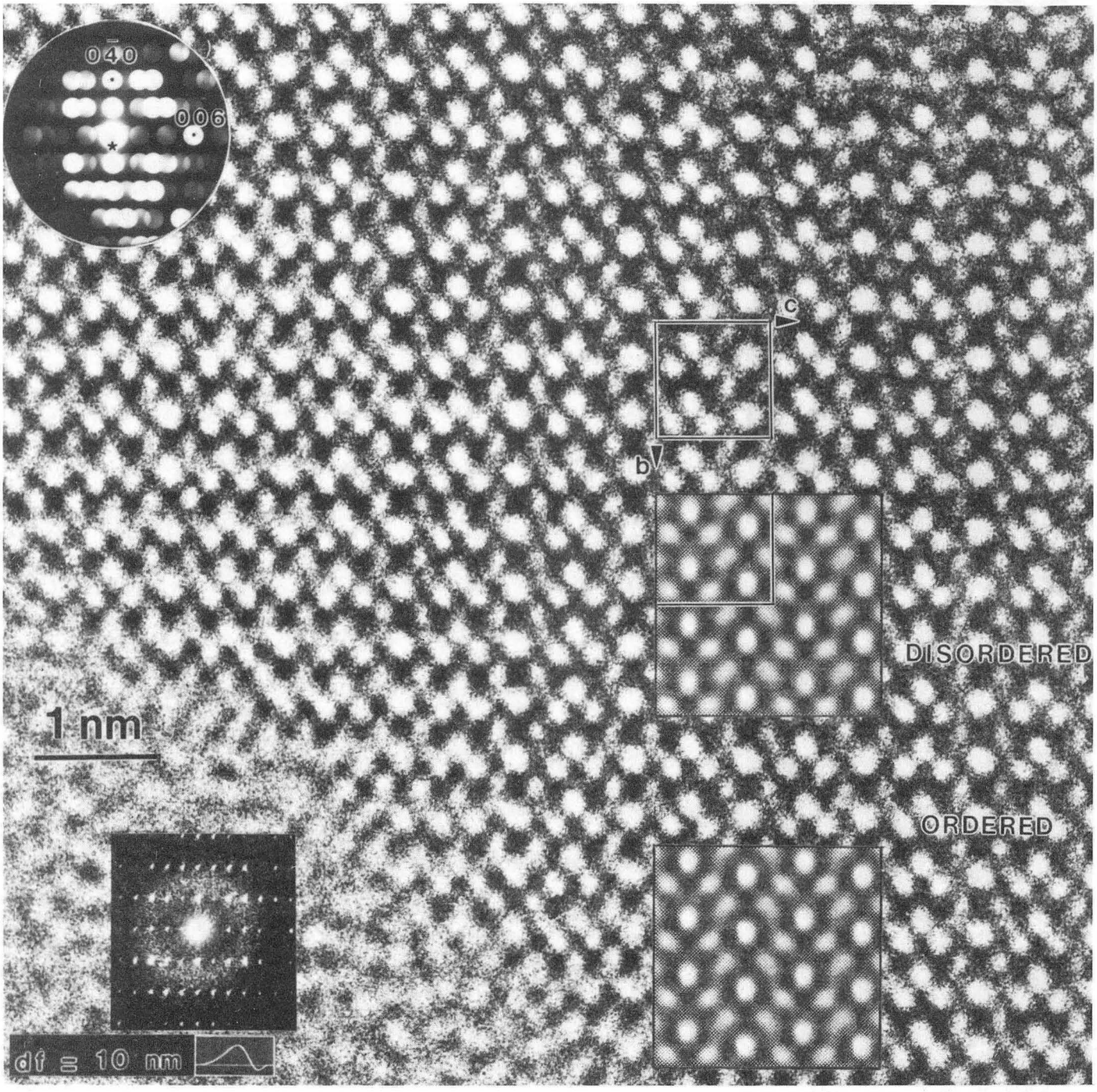

XBB 902-1488

Fig. 3

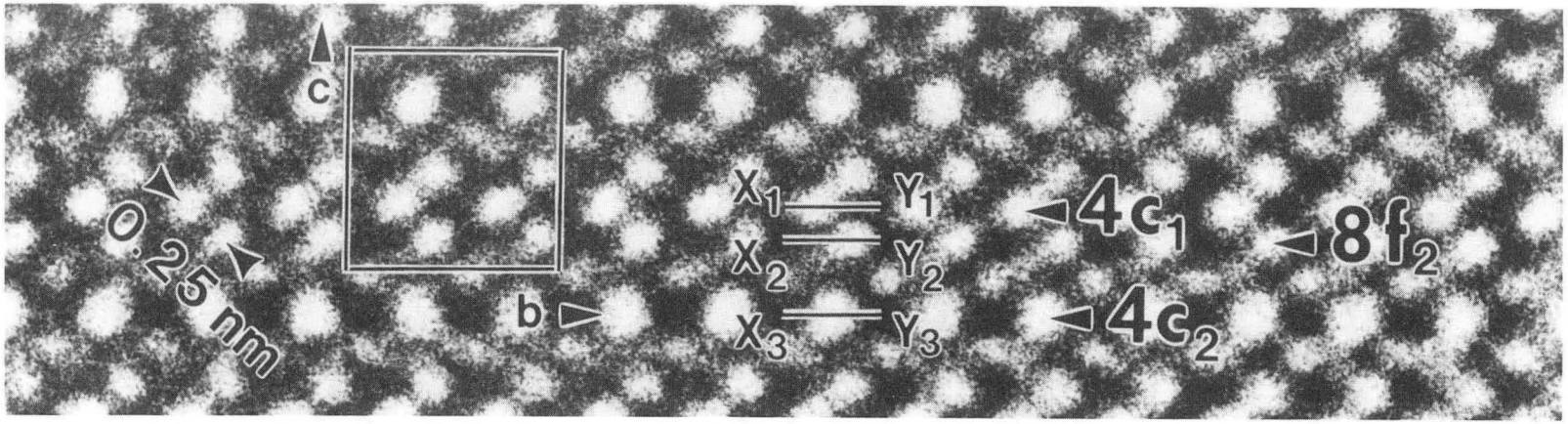

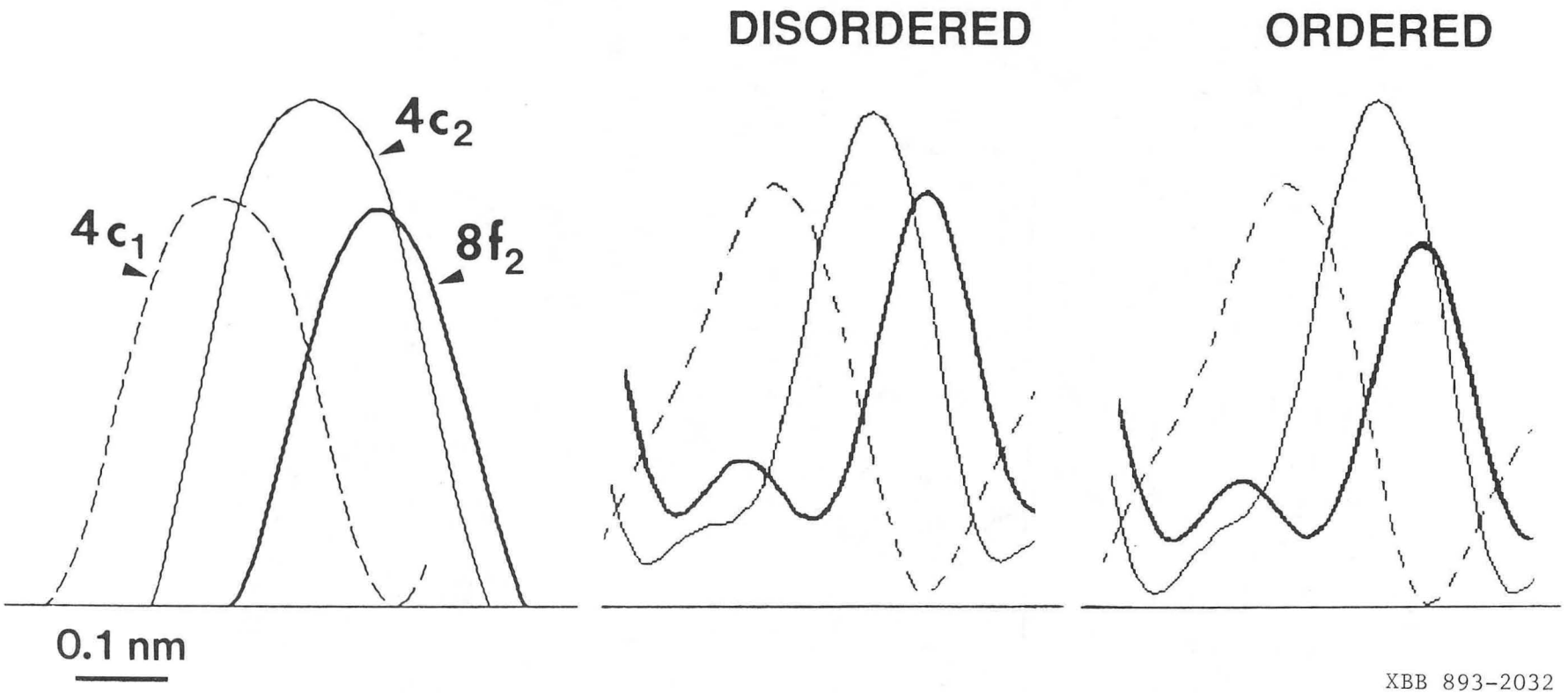

XBB 893-2032

Fig. 4

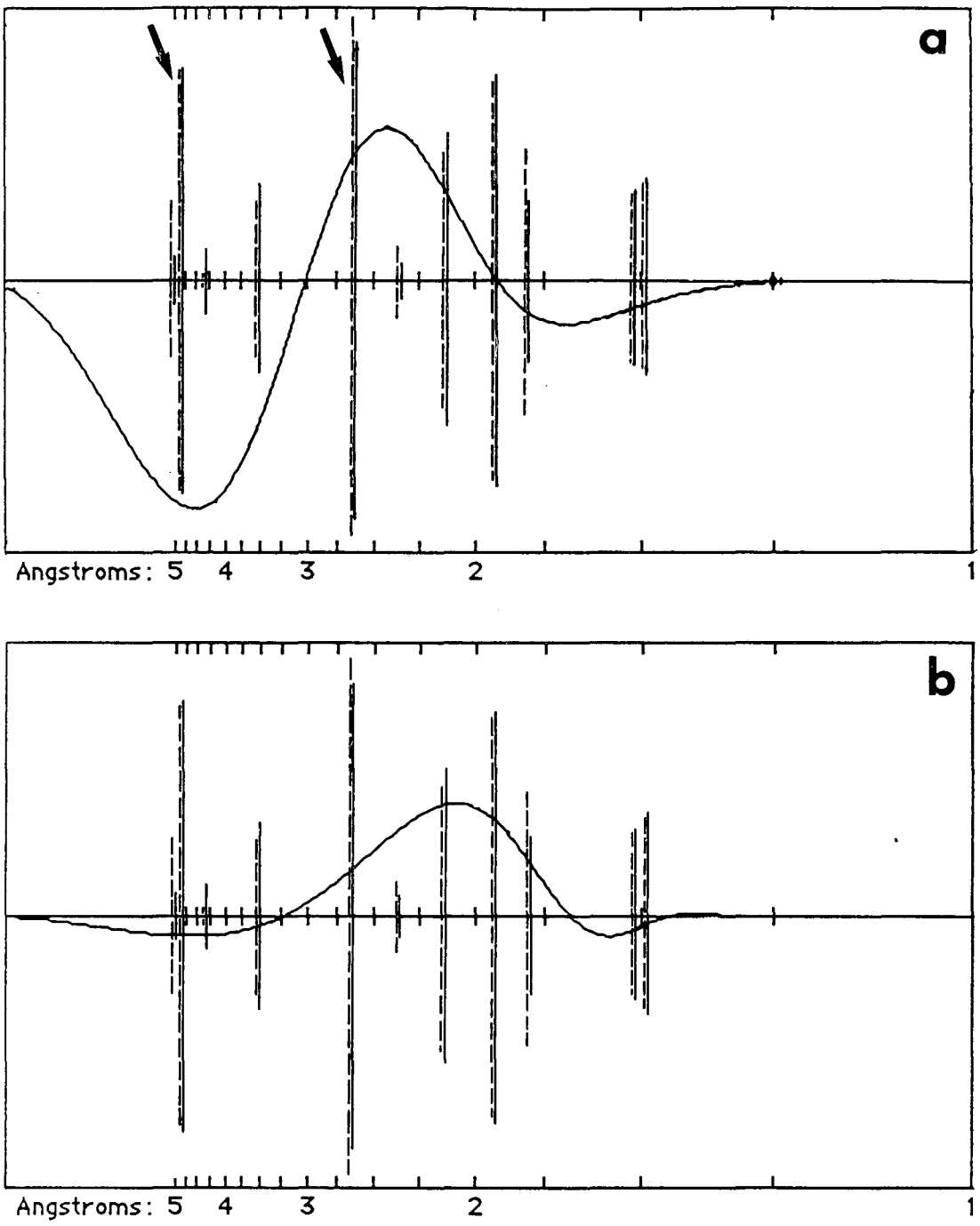

XBL 902-649

Fig. 5

LAWRENCE BERKELEY LABORATORY
TECHNICAL INFORMATION DEPARTMENT
1 CYCLOTRON ROAD
BERKELEY, CALIFORNIA 94720